ARTICLE

Check for updates

Symmetry-protected difference between spin Hall and anomalous Hall effects of a periodically driven multiorbital metal

Naoya Arakawa [1]✉ & Kenji Yonemitsu [1,2]

Nonequilibrium quantum states can be controlled via the driving field in periodically driven systems. Such control, which is called Floquet engineering, has opened various phenomena, such as the light-induced anomalous Hall effect. There are expected to be some essential differences between the anomalous Hall and spin Hall effects of periodically driven systems because of the difference in time-reversal symmetry. However, these differences remain unclear due to the lack of Floquet engineering of the spin Hall effect. Here we show that when the helicity of circularly polarized light is changed in a periodically driven t_{2g}-orbital metal, the spin current generated by the spin Hall effect remains unchanged, whereas the charge current generated by the anomalous Hall effect is reversed. This difference is protected by the symmetry of a time reversal operation. Our results offer a way to distinguish the spin current and charge current via light and could be experimentally observed in pump-probe measurements of periodically driven Sr_2RuO_4.

[1] The Institute of Science and Engineering, Chuo University, Bunkyo, Tokyo 112-8551, Japan. [2] Department of Physics, Chuo University, Bunkyo, Tokyo 112-8551, Japan. ✉email: arakawa@phys.chuo-u.ac.jp

P eriodically driven systems enable the realization of various nonequilibrium quantum states and their control. Periodically driven systems are realized by a time-periodic field, and their properties in a nonequilibrium steady state can be described by the Floquet theory[1–5], in which the effective Hamiltonian is independent of time. In fact, various theoretical predictions, such as the light-induced anomalous-Hall effect (AHE)[6–8] and the Floquet time crystal[9–11], are confirmed by experiments. Then, since the effective Hamiltonian of the Floquet theory depends on parameters of the driving field, its properties can be controlled by tuning the driving field. This is called Floquet engineering[3–5]. For example, it is possible to change the magnitude, sign, and bond anisotropy of exchange interactions of Mott insulators[12–16]. The Floquet engineering has been studied in many fields of physics, including condensed-matter, cold-atom, and optical physics.

Although there are many studies of the AHE of periodically driven systems, the Floquet engineering of the spin-Hall effect (SHE) is still lacking. The SHE is the key phenomenon in spintronics[17–21]. In the SHE, an electron spin current, a flow of the spin angular momentum, is generated by an electric field perpendicular to it[22–24]. This is the spin version of the AHE, in which an electron charge current is generated[25,26]. A significant difference between the AHE and SHE is about time-reversal symmetry (TRS): TRS is broken in the AHE, whereas it holds in the SHE. Since TRS can be broken by circularly polarized light[27], there should be some essential differences between those of a periodically driven system. It is highly desirable to investigate the intrinsic SHE of a periodically driven multiorbital metal because the intrinsic SHE, the SHE intrinsic to the electronic structure, can be engineered by the driving field and several multiorbital metals, such as Pt, have the huge SHE[28,29].

Here we show that in a multiorbital metal driven by circularly polarized light, the charge current generated by the AHE can be reversed by changing the helicity of light, whereas the spin current generated by the SHE remains unchanged. This is demonstrated by constructing a theory of pump-probe measurements of the AHE and SHE of a periodically driven t_{2g}-orbital metal coupled to a heat bath and evaluating their conductivities numerically. This significant difference between the AHE and SHE results from the difference in TRS and thus should hold in many periodically driven systems. We also show that spin–orbit coupling (SOC) is vital for the SHE of the periodically driven multiorbital metal, whereas it is unnecessary for the AHE. This property is distinct from that of non-driven metals.

Results and discussion
Periodically driven t_{2g}-orbital metal. We consider a t_{2g}-orbital metal coupled to a heat bath in the presence of a field $\mathbf{A}(t)$ (Fig. 1a):

$$H(t) = H_s(t) + H_{sb} + H_b. \tag{1}$$

(Note that in the t_{2g}-orbital metal, such as Sr_2RuO_4, electrons occupy the t_{2g} orbitals, i.e., the d_{yz}, d_{zx}, and d_{xy} orbitals). First, $H_s(t)$ is the system Hamiltonian, the Hamiltonian of t_{2g}-orbital electrons with $\mathbf{A}(t)$,

$$H_s(t) = \sum_{\mathbf{k}} \sum_{a,b=d_{yz},d_{zx},d_{xy}} \sum_{\sigma,\sigma'=\uparrow,\downarrow} \bar{\epsilon}_{ab}^{\sigma\sigma'}(\mathbf{k},t) c_{\mathbf{k}a\sigma}^{\dagger} c_{\mathbf{k}b\sigma'}. \tag{2}$$

Here $c_{\mathbf{k}a\sigma}^{\dagger}$ and $c_{\mathbf{k}a\sigma}$ are the creation and annihilation operators, respectively, of an electron for orbital a with momentum $\mathbf{k}$ and spin σ, and

$$\bar{\epsilon}_{ab}^{\sigma\sigma'}(\mathbf{k},t) = [\epsilon_{ab}(\mathbf{k},t) - \mu\delta_{a,b}]\delta_{\sigma,\sigma'} + \xi_{ab}^{\sigma\sigma'}, \tag{3}$$

where $\epsilon_{ab}(\mathbf{k},t)$, μ, and $\xi_{ab}^{\sigma\sigma'}$ are the kinetic energy with the Peierls

phase factors due to $\mathbf{A}(t)$, the chemical potential, and SOC, respectively (see Methods). Throughout this paper, we use the unit $\hbar = 1$, $k_B = 1$, and $a_{lc} = 1$, where a_{lc} is the lattice constant. In addition to $H_s(t)$, we have considered H_b and H_{sb}, the Hamiltonian of a Büttiker-type heat bath[30–33] at temperature T_b and the system-bath coupling Hamiltonian (see Methods). This is because a nonequilibrium steady state can be realized due to the damping coming from the second-order perturbation of H_{sb}[32,34].

The parameters of $H_s(t)$ are chosen to reproduce the electronic structure of Sr_2RuO_4[35]. The hopping integrals on the square lattice are parametrized by t_1, t_2, t_3, t_4, and t_5 (Fig. 1b)[36], and μ is determined from the condition $n_e = 4$, where n_e is the electron number per site; the value of μ is fixed at that determined in the non-driven case. We set $(t_1, t_2, t_3, t_4, t_5) = (0.675, 0.09, 0.45, 0.18, 0.03)$ (eV)[36] and $\xi = 0.17$ eV[37], where ξ is the coupling constant of SOC, in order that the Fermi surface (Fig. 1c) is consistent with that observed experimentally[38].

Theory of pump-probe measurements of the SHE and AHE. The SHE and AHE of a periodically driven system are detectable by pump-probe measurements. In the pump-probe measurements[39], a system is periodically driven by the pump field $\mathbf{A}_{pump}(t)$, and its properties are analyzed by the probe field $\mathbf{A}_{prob}(t)$. Thus, we set $\mathbf{A}(t) = \mathbf{A}_{pump}(t) + \mathbf{A}_{prob}(t)$ and treat the effects of $\mathbf{A}_{pump}(t)$ in the Floquet theory and those of $\mathbf{A}_{prob}(t)$ in the linear-response theory[33,40]; in our analyses, $\mathbf{A}_{pump}(t)$ is chosen to be

$$\mathbf{A}_{pump}(t) = {}^t(A_0 \cos\Omega t \; A_0 \sin(\Omega t + \delta)), \tag{4}$$

where $\Omega = 2\pi/T$ and T is the period of $\mathbf{A}_{pump}(t)$. The anomalous-Hall and spin-Hall conductivities $\sigma_{yx}^C(t,t')$ and $\sigma_{yx}^S(t,t')$ are defined as

$$\sigma_{yx}^Q(t,t') = \frac{1}{i\omega} \frac{\delta\langle j_Q^y(t)\rangle}{\delta A_{prob}^x(t')}, \tag{5}$$

where $\langle j_C^y(t)\rangle$ and $\langle j_S^y(t)\rangle$ are the expectation values of the charge and spin current density operators, respectively. In our AHE or SHE, we have considered the charge or spin current, respectively, generated along the y-axis with the probe field applied along the x-axis (Fig. 1a). (Note that our SHE is different from the SHE of light, in which the helicity-dependent transverse shift of light at an interface is induced[41–43]). Then, the charge and spin current operators $J_C^y(t) = Nj_C^y(t)$ and $J_S^y(t) = Nj_S^y(t)$, where N is the number of sites, are determined from the continuity equations (see Methods)[28,29,44,45]:

$$J_Q^y(t) = \sum_{\mathbf{k}} \sum_{a,b} \sum_{\sigma} v_{ab\sigma}^{(Q)y}(\mathbf{k},t) c_{\mathbf{k}a\sigma}^{\dagger}(t) c_{\mathbf{k}b\sigma}(t), \tag{6}$$

where $v_{ab\sigma}^{(C)y}(\mathbf{k},t) = (-e)\frac{\partial\epsilon_{ab}(\mathbf{k},t)}{\partial k_y}$, $v_{ab\sigma}^{(S)y}(\mathbf{k},t) = \frac{1}{2}\text{sgn}(\sigma)\frac{\partial\epsilon_{ab}(\mathbf{k},t)}{\partial k_y}$, and $\text{sgn}(\sigma) = 1$ or -1 for $\sigma = \uparrow$ or $\downarrow$, respectively. By combining Eq. (6) with Eq. (5) and using a method of Green's functions[34,44,46,47], we can express $\sigma_{yx}^Q(t,t')$ in terms of electron Green's functions (see Methods).

To analyze the SHE and AHE in the nonequilibrium steady state, we consider the time-averaged dc anomalous-Hall and spin-Hall conductivities σ_{yx}^C and σ_{yx}^S,

$$\sigma_{yx}^Q = \lim_{\omega\to 0} \text{Re} \int_0^T \frac{dt_{av}}{T} \int_{-\infty}^{\infty} dt_{rel} e^{i\omega t_{rel}} \sigma_{yx}^Q(t,t'), \tag{7}$$

where $t_{rel} = t - t'$ and $t_{av} = (t + t')/2$[33]. Since we can calculate Eq. (7) in a way similar to that for charge transport of single-orbital systems[32,33,40], we present the final result here (for the
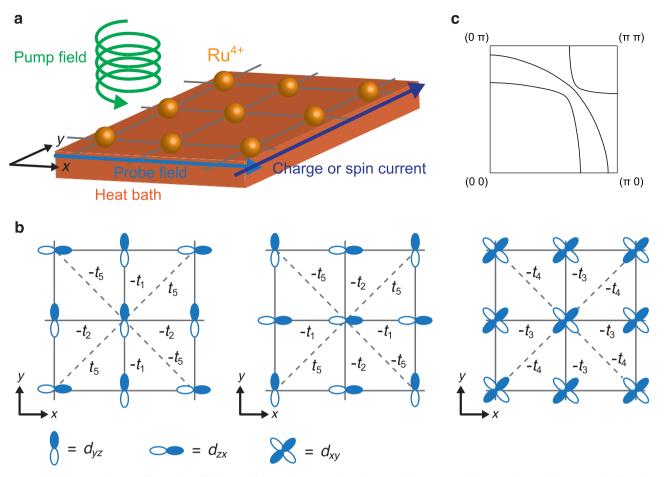
Fig. 1 Set-up of the anomalous-Hall or spin-Hall effect and electronic properties of our model. a Set-up of the anomalous-Hall or spin-Hall effect for our model of Sr$_2$RuO$_4$ driven by circularly polarized light in the presence of the coupling to a heat bath. In Sr$_2$RuO$_4$, Ru ions form the square lattice; at each ion, four electrons occupy the Ru t_{2g} orbitals (i.e., the d_{yz}, d_{zx}, and d_{xy} orbitals). In the pump-probe measurements of the anomalous-Hall and spin-Hall effects, the probe field induces the charge and spin currents, respectively, perpendicular to it, and the pump field, a field of left- or right-circularly polarized light, periodically drives Sr$_2$RuO$_4$. The nonequilibrium steady state is realized because of the coupling to the heat bath. **b** The finite hopping processes of electrons in t_{2g} orbitals on the square lattice. The d_{yz}, d_{zx}, and d_{xy} represent these orbitals. t_1, t_2, and t_3 are the nearest-neighbor hopping integrals, and t_4 and t_5 are the next nearest-neighbor ones. **c** The Fermi surface obtained for the non-driven case of our model in the quarter of the Brillouin zone. The other parts are reproducible by using the rotational symmetry.

derivation, see Supplementary Note 1):

$$\sigma_{yx}^{Q} = \frac{1}{N} \sum_{\mathbf{k}} \sum_{a,b,c,d} \sum_{\sigma,\sigma'} \int_{-\Omega/2}^{\Omega/2} \frac{d\omega'}{2\pi} \sum_{m,l,n,q=-\infty}^{\infty} [v_{ab\sigma}^{(Q)y}(\mathbf{k})]_{ml}$$

$$\times [v_{cd\sigma'}^{(C)x}(\mathbf{k})]_{nq} \left\{ \frac{\partial [G_{b\sigma c\sigma'}^{R}(\mathbf{k},\omega')]_{ln}}{\partial \omega'} [G_{d\sigma'a\sigma}^{<}(\mathbf{k},\omega')]_{qm} \right. \quad (8)$$

$$\left. - [G_{b\sigma c\sigma'}^{<}(\mathbf{k},\omega')]_{ln} \frac{\partial [G_{d\sigma'a\sigma}^{A}(\mathbf{k},\omega')]_{qm}}{\partial \omega'} \right\},$$

where $[v_{ab\sigma}^{(Q)\nu}(\mathbf{k})]_{mn}$ (Q = C or S, $\nu = y$ or x) and $[G_{a\sigma b\sigma'}^{r}(\mathbf{k},\omega')]_{mn}$ (r = R, A, or <) are given by

$$[v_{ab\sigma}^{(Q)\nu}(\mathbf{k})]_{mn} = \int_0^T \frac{dt}{T} e^{i(m-n)\Omega t} v_{ab\sigma}^{(Q)\nu}(\mathbf{k},t), \quad (9)$$

$$\left[G_{a\sigma b\sigma'}^{r}(\mathbf{k},\omega') \right]_{mn} = \int_{-\infty}^{\infty} dt_{rel} e^{i(\omega' + \frac{m+n}{2}\Omega)t_{rel}} \int_0^T \frac{dt_{av}}{T} \quad (10)$$

$$\times e^{i(m-n)\Omega t_{av}} G_{a\sigma b\sigma'}^{r}(\mathbf{k};t,t'),$$

respectively; the three Green's functions are determined from the Dyson equation with the damping Γ due to the system-bath

coupling (see Methods). (For the energy dispersion of our model, see Supplementary Note 2.)

Helicity-independent σ_{yx}^{S} and helicity-dependent σ_{yx}^{C}. We evaluate σ_{yx}^{C} and σ_{yx}^{S} numerically. (For the details of the numerical calculations, see Methods.) We set $\Gamma = 0.03$ eV and $T_b = 0.05$ eV; Γ is chosen to be smaller than T_b because the system is supposed to be well described by the Fermi liquid. To study how σ_{yx}^{C} and σ_{yx}^{S} are affected by the helicity of light, we consider the $\mathbf{A}_{pump}(t)$'s for $\delta = 0$ and π [Eq. (4)], $\mathbf{A}_{LCP}(t)$ and $\mathbf{A}_{RCP}(t)$, which correspond to the cases of the left- and right-circularly polarized light, respectively. We show how σ_{yx}^{S} and σ_{yx}^{C} depend on a dimensionless quantity $u = eA_0 = eE_0/\Omega$. Note that the u dependence at fixed Ω corresponds to the dependence on E_0, the amplitude of the electric field.

σ_{yx}^{S} and σ_{yx}^{C} have the different helicity dependences. Figure 2a shows the dependence of σ_{yx}^{S} on $u = eA_0$ for $\mathbf{A}_{pump}(t) = \mathbf{A}_{LCP}(t)$ or $\mathbf{A}_{RCP}(t)$ at $\Omega = 6$ eV. The σ_{yx}^{S} for $\mathbf{A}_{pump}(t) = \mathbf{A}_{LCP}(t)$ is the same as that for $\mathbf{A}_{pump}(t) = \mathbf{A}_{RCP}(t)$. This property holds even at $\Omega = 4$ and 2 eV (Fig. 2b, c). Note that $\Omega = 6$, 4, and 2 eV correspond to $\Omega > W$, $\Omega \approx W$, and $\Omega < W$, respectively, where $W(\approx 4\text{eV})$ is the bandwidth in the non-driven case. Meanwhile,
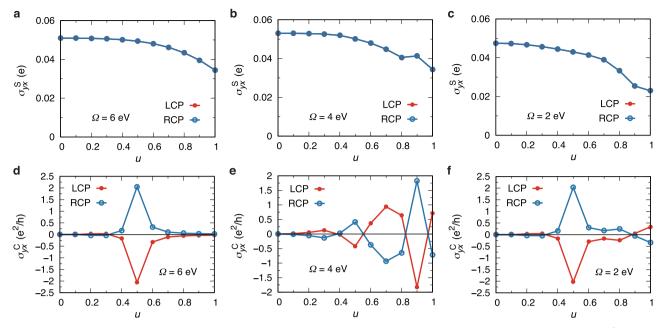
Fig. 2 Helicity dependences of the spin-Hall and anomalous-Hall conductivities. a, b, c The dependences of the spin-Hall conductivity σ_{yx}^{S} on the dimensionless quantity $u = eA_0$ in the case of left- or right-circularly polarized light (LCP or RCP) at $\Omega = 6$, 4, and 2 eV, where Ω is the frequency of light. The red and blue curves correspond to those in the case of left- or right-circularly polarized light, respectively. **d, e, f** The dependences of the anomalous-Hall conductivity σ_{yx}^{C} on $u = eA_0$ in the case of left- or right-circularly polarized light at $\Omega = 6$, 4, and 2 eV. The same notations as those in **a, b, c** are used.
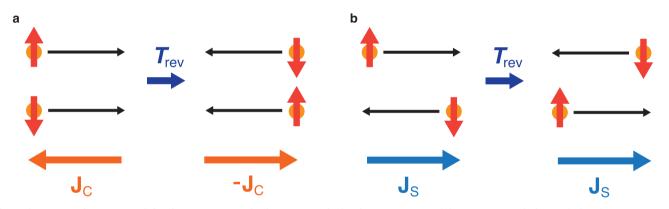

Fig. 3 Time-reversal symmetry of the charge current and spin current. a, b The charge currents and the spin currents before and after the time-reversal operation T_{rev}. The charge current $\mathbf{J}_C$ and the spin current $\mathbf{J}_S$ are $\mathbf{J}_C = (-e)(\mathbf{J}_\uparrow + \mathbf{J}_\downarrow)$ and $\mathbf{J}_S = (1/2)(\mathbf{J}_\uparrow - \mathbf{J}_\downarrow)$, where $\mathbf{J}_\uparrow$ and $\mathbf{J}_\downarrow$ are the spin-up and spin-down electron currents, respectively. As a result of T_{rev}, $\mathbf{J}_\uparrow$ and $\mathbf{J}_\downarrow$ become $-\mathbf{J}_\downarrow$ and $-\mathbf{J}_\uparrow$, respectively. Thus, $\mathbf{J}_C$ changes its sign (**a**), whereas $\mathbf{J}_S$ remains the same (**b**). Namely, $\mathbf{J}_C$ breaks time-reversal symmetry, but $\mathbf{J}_S$ does not.

σ_{yx}^{C}'s for $\mathbf{A}_{pump}(t) = \mathbf{A}_{LCP}(t)$ and $\mathbf{A}_{RCP}(t)$ are opposite in sign and the same in magnitude at $\Omega = 6$, 4, and 2 eV (Fig. 2d–f). Although such helicity-dependent σ_{yx}^{C} was experimentally shown in graphene[8], its origin may be unexplored. Note that the difference between the u dependences of σ_{yx}^{S} and σ_{yx}^{C} can be qualitatively understood by considering the dominant terms of the Bessel functions due to the Peierls phase factors (see Supplementary Note 3 and Supplementary Fig. 1).

This difference between σ_{yx}^{S} and σ_{yx}^{C} comes from the difference in TRS. Under the time-reversal operation T_{rev}, time t, momentum $\mathbf{k}$, and spin σ are changed as follows: $(t, \mathbf{k}, \sigma) \rightarrow (-t, -\mathbf{k}, -\sigma)$, where $-\sigma = \downarrow$ or $\uparrow$ for $\sigma = \uparrow$ or $\downarrow$, respectively. The spin current and charge current are expressed as $\mathbf{J}_S = \frac{1}{2}(\mathbf{J}_\uparrow - \mathbf{J}_\downarrow)$ and $\mathbf{J}_C = (-e)(\mathbf{J}_\uparrow + \mathbf{J}_\downarrow)$, where $\mathbf{J}_\uparrow$ and $\mathbf{J}_\downarrow$ are the contributions from the spin-up and spin-down electrons, respectively. Thus, $(\mathbf{J}_S, \mathbf{J}_C) \rightarrow (\mathbf{J}_S, -\mathbf{J}_C)$ is obtained as a result of T_{rev} because $(\mathbf{J}_\uparrow, \mathbf{J}_\downarrow) \rightarrow (-\mathbf{J}_\downarrow, -\mathbf{J}_\uparrow)$ is satisfied under T_{rev} (Fig. 3a, b). (This is

the reason why TRS is broken in the AHE and not broken in the SHE.) Meanwhile, the right- and left-circularly polarized light fields are connected by T_{rev} because $\mathbf{A}_{RCP}(-t) = \mathbf{A}_{LCP}(t)$. Namely, replacing $\mathbf{A}_{LCP}(t)$ by $\mathbf{A}_{RCP}(t)$ corresponds to applying T_{rev}. Thus, the helicity-independent σ_{yx}^{S} and the helicity-dependent σ_{yx}^{C} result from $\mathbf{J}_S \rightarrow \mathbf{J}_S$ and $\mathbf{J}_C \rightarrow -\mathbf{J}_C$, respectively, under T_{rev}.

The same helicity dependences hold in many periodically driven multiorbital metals. The spin current and charge current are of the same form for some transition metals (e.g., Pt and Au)[28] and transition-metal oxides. Then, the similar SHE and AHE can be realized using circularly polarized light. Thus, the above arguments are applicable to many transition-metal oxides and transition metals driven by circularly polarized light.

SOC-dependent σ_{yx}^{S} and SOC-independent σ_{yx}^{C}. There is another difference between σ_{yx}^{S} and σ_{yx}^{C}. Figure 4a compares the u dependence of σ_{yx}^{S} with SOC to that without SOC. In the absence
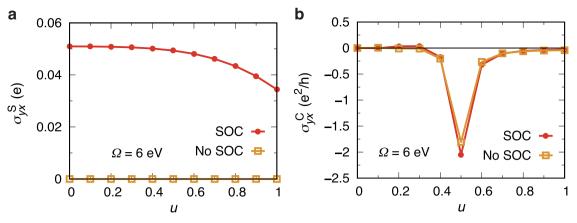
Fig. 4 Spin–orbit coupling dependences of the spin-Hall and anomalous-Hall conductivities. a, b The dependences of the spin-Hall and anomalous-Hall conductivities σ_{yx}^{S} and σ_{yx}^{C} on the dimensionless quantity $u = eA_0$ in the case of left-circularly polarized light at $\Omega = 6$ eV with and without spin–orbit coupling. Here Ω is the frequency of light. The red and yellow curves correspond to those with and without spin–orbit coupling, respectively.

of SOC, $\sigma_{yx}^{S} = 0$. This is because there is no spin-dependent term in the Hamiltonian except for SOC. The spin-dependent term, such as SOC, is needed to obtain the finite difference between the spin-up and spin-down electron currents. Meanwhile, the u dependence of σ_{yx}^{C} with SOC is almost the same as that without SOC (Fig. 4b). This is because a spin-independent electron current can be generated by using the kinetic energy terms with the Peierls phase factors[6,33] and a multiorbital mechanism[48] using SOC does not contribute to σ_{yx}^{C} in the presence of spin degeneracy, which is not lifted by the Peierls phase factors. Note that in periodically driven systems, σ_{yx}^{C} can be finite even without orbital degrees of freedom[6,33] because the Peierls phase factors can lead to the terms odd with respect to momentum in the energy dispersion (see Supplementary Note 2).

These results suggest that in periodically driven multiorbital metals, SOC is vital for the SHE, whereas it is unnecessary for the AHE. This suggestion may be valid as long as the effects of the driving field can be treated as the Peierls phase factors and there is no magnetic order. In addition, this is distinct from the property of non-driven multiorbital metals where SOC is vital for the SHE and AHE[24–26,28,29,48]. In contrast, the multiorbital nature is required for the SHE of periodically driven systems, whereas it is unnecessary for the AHE.

Implications and experimental realization. We discuss some implications of our results. First, the difference between the helicity dependences of σ_{yx}^{S} and σ_{yx}^{C} can be used to distinguish the spin current and charge current without ambiguity. Since that difference results from the symmetry of T_{rev}, the same helicity dependences should hold in many periodically driven systems. In addition, the similar arguments enable us to distinguish two currents, one of which breaks TRS (and the other does not), in not only Hall effects, but also other transport phenomena. Thus, our results have revealed the core physics discipline about the relations between TRS and transport properties of periodically driven systems. Then, our theory can be extended to the SHE and AHE of other multiorbital metals and other transport phenomena. For example, a combination of it and first-principles calculations enables us to systematically search the SHE and AHE of periodically driven multiorbital metals. Thus, our results provide the first step towards the Floquet engineering of spintronics phenomena, including the SHE, of periodically driven multiorbital metals.

Finally, we comment on experimental realization. In our theory, interaction effects and heating effects are neglected. For

Sr$_2$RuO$_4$, electron-electron interactions cause the orbital-dependent damping and mass enhancement[35,49]. Since these effects are quantitative[29], the interaction effects may not change our results at least qualitatively. The differences in the helicity dependence and the SOC dependence will hold because those interaction effects do not break TRS. In general, the periodic driving makes the system to heat up[50]. However, for the periodically driven open system, such as our system, a nonequilibrium steady state can be realized due to Γ[32,33,51] at times larger than $\tau(= \hbar/2\Gamma) \approx 11$fs $= O(10$fs$)$. In fact, the AHE predicted theoretically in a periodically driven open system[6] is experimentally realized[7,8]. For Sr$_2$RuO$_4$, in which $a_{lc} \approx 0.39$ nm[35], $u(= ea_{lc}A_0) = 0.3$ at $\Omega = 2$, 4, or 6 eV corresponds to $E_0 = A_0/\Omega \approx 15$, 31, or 46 MVcm^{-1}, respectively. Since the pump field of the order of 10 MVcm^{-1} is experimentally accessible[52], we conclude that the predicted properties of σ_{yx}^{S} and σ_{yx}^{C} could be observed in the pump-probe measurements of the SHE and AHE in periodically driven Sr$_2$RuO$_4$.

Methods

Tight-binding Hamiltonian with SOC. We have chosen the following tight-binding Hamiltonian for t_{2g}-orbital electrons as $H_s(t)$:

$$H_s(t) = \sum_{i,j} \sum_{a,b=d_{yz},d_{zx},d_{xy}} \sum_{\sigma=\uparrow,\downarrow} [t_{ij}^{ab}(t) - \mu\delta_{i,j}\delta_{a,b}]c_{ia\sigma}^{\dagger}c_{jb\sigma}$$
$$+ \sum_{i} \sum_{a,b=d_{yz},d_{zx},d_{xy}} \sum_{\sigma,\sigma'=\uparrow,\downarrow} \xi_{ab}^{\sigma\sigma'} c_{ia\sigma}^{\dagger}c_{ib\sigma'}, \quad (11)$$

where $t_{ij}^{ab}(t)$'s are the hopping integrals with the Peierls phase factors due to $\mathbf{A}(t)$, $t_{ij}^{ab}(t) = t_{ij}^{ab}e^{-ie(\mathbf{R}_i-\mathbf{R}_j)\cdot\mathbf{A}(t)}$, and $\xi_{ab}^{\sigma\sigma'}$ is the coupling constant of the SOC for t_{2g}-orbital electrons. The finite elements of $\xi_{ab}^{\sigma\sigma'} = (\xi_{ba}^{\sigma'\sigma})^*$ are given by $\xi_{d_{yz}d_{zx}}^{\uparrow\uparrow} = \xi_{d_{zx}d_{yz}}^{\downarrow\downarrow} = i\xi/2$, $\xi_{d_{zx}d_{xy}}^{\uparrow\downarrow} = -\xi/2$, $\xi_{d_{xy}d_{yz}}^{\uparrow\downarrow} = \xi/2$, and $\xi_{d_{xy}d_{zx}}^{\downarrow\downarrow} = \xi_{d_{yz}d_{zx}}^{\downarrow\downarrow} = -i\xi/2$. By using the Fourier coefficients of the operators, we can write Eq. (11) as Eq. (2) with Eq. (3), in which $\epsilon_{ab}(\mathbf{k}, t)$ is given by $\epsilon_{ab}(\mathbf{k}, t) = \sum_j t_{ij}^{ab}(t)e^{-i\mathbf{k}\cdot(\mathbf{R}_i-\mathbf{R}_j)}$.

Büttiker-type heat bath. H_{sb} and H_b in Eq. (1) are given by

$$H_{sb} = \sum_i \sum_p \sum_{a=d_{yz},d_{zx},d_{xy}} \sum_{\sigma=\uparrow,\downarrow} V_{pa\sigma}(c_{ia\sigma}^{\dagger}b_{ip} + b_{ip}^{\dagger}c_{ia\sigma}), \quad (12)$$

$$H_b = \sum_i \sum_p (\epsilon_p - \mu_b)b_{ip}^{\dagger}b_{ip}, \quad (13)$$

where b_{ip} and $b_{ip}^{\dagger}$ are the annihilation and creation operators, respectively, of a bath's fermion at site i for mode p, $V_{pa\sigma}$ is the coupling constant, and ϵ_p and μ_b are the energy and chemical potential of a bath's fermion. Note that μ_b is chosen in order that there is no current between the system and bath. The heat bath is supposed to be in equilibrium at temperature T_b. The main effect of the heat bath is the damping appearing in electron Green's functions[32,33].

Charge current and spin current operators. We derive the charge current and spin current operators using the continuity equations. Theories using these operators derived in that way succeed in describing the SHE observed in non-driven multiorbital metals[28,53].

First, we derive the charge current operator $\mathbf{J}_C(t)$. $\mathbf{J}_C(t)$ is supposed to satisfy the continuity equation[44],

$$\frac{d\rho_j(t)}{dt} + \nabla \cdot \mathbf{j}_j^{(C)}(t) = 0, \tag{14}$$

where $\rho_j(t) = (-e)\sum_a \sum_\sigma c_{ja\sigma}^\dagger(t)c_{ja\sigma}(t)$ and $\sum_j \mathbf{j}_j^{(C)}(t) = \mathbf{J}_C(t)$. Using Eq. (14), we have

$$\sum_j \mathbf{R}_j \frac{d\rho_j(t)}{dt} = -\sum_j \mathbf{R}_j \nabla \cdot \mathbf{j}_j^{(C)}(t) = \mathbf{J}_C(t), \tag{15}$$

where we have omitted the surface contributions. By combining it with the Heisenberg equation, we can write Eq. (15) as

$$\mathbf{J}_C(t) = i[H_s(t), \sum_j \mathbf{R}_j \rho_j(t)]. \tag{16}$$

(Note that there is no contribution from H_{sb} because the bath's chemical potential is chosen in order that there is no current between the system and bath). After some calculations, we obtain

$$\mathbf{J}_C(t) = i\sum_{i,j}\sum_{a,b}\sum_\sigma (-e)t_{ij}^{ab}(t)(\mathbf{R}_j - \mathbf{R}_i)c_{ia\sigma}^\dagger(t)c_{jb\sigma}(t)$$
$$= -e\sum_{\mathbf{k}}\sum_{a,b}\sum_\sigma \frac{\partial \epsilon_{ab}(\mathbf{k}, t)}{\partial \mathbf{k}}c_{\mathbf{k}a\sigma}^\dagger(t)c_{\mathbf{k}b\sigma}(t). \tag{17}$$

Similarly, we derive the spin current operator $\mathbf{J}_S(t)$. We suppose that $\mathbf{J}_S(t)$ satisfies

$$\frac{dS_j^z(t)}{dt} + \nabla \cdot \mathbf{j}_j^{(S)}(t) = 0, \tag{18}$$

where $S_j^z(t) = \sum_a \sum_\sigma \frac{1}{2}\text{sgn}(\sigma)c_{ja\sigma}^\dagger(t)c_{ja\sigma}(t)$ and $\sum_j \mathbf{j}_j^{(S)}(t) = \mathbf{J}_S(t)$. In a way similar to the derivation of $\mathbf{J}_C(t)$, $\mathbf{J}_S(t)$ is given by

$$\mathbf{J}_S(t) = i[H_s(t), \sum_j \mathbf{R}_j S_j^z(t)]$$
$$= \frac{1}{2}\sum_{\mathbf{k}}\sum_{a,b}\sum_\sigma \text{sgn}(\sigma)\frac{\partial \epsilon_{ab}(\mathbf{k}, t)}{\partial \mathbf{k}}c_{\mathbf{k}a\sigma}^\dagger(t)c_{\mathbf{k}b\sigma}(t). \tag{19}$$

Anomalous-Hall and spin-Hall conductivities as functions of time. We express $\sigma_{yx}^C(t, t')$ and $\sigma_{yx}^S(t, t')$ in terms of the electron Green's functions. Using Eq. (6), we have

$$\langle j_C^y(t)\rangle = \frac{-i}{N}\sum_{\mathbf{k}}\sum_{a,b}\sum_\sigma v_{ab\sigma}^{(C)y}(\mathbf{k}, t)G_{b\sigma a\sigma}^<(\mathbf{k}; t, t), \tag{20}$$

$$\langle j_S^y(t)\rangle = \frac{-i}{N}\sum_{\mathbf{k}}\sum_{a,b}\sum_\sigma v_{ab\sigma}^{(S)y}(\mathbf{k}, t)G_{b\sigma a\sigma}^<(\mathbf{k}; t, t), \tag{21}$$

where $G_{b\sigma'a\sigma}^<(\mathbf{k}; t, t')$ is the lesser Green's function[34,44,46,47],

$$G_{b\sigma'a\sigma}^<(\mathbf{k}; t, t') = i\langle c_{\mathbf{k}a\sigma}^\dagger(t')c_{\mathbf{k}b\sigma'}(t)\rangle. \tag{22}$$

By substituting Eqs. (20) and (21) into Eq. (5), we can express $\sigma_{yx}^C(t, t')$ and $\sigma_{yx}^S(t, t')$ as follows:

$$\sigma_{yx}^C(t, t') = \sigma_{yx}^{C(1)}(t, t') + \sigma_{yx}^{C(2)}(t, t'), \tag{23}$$

$$\sigma_{yx}^S(t, t') = \sigma_{yx}^{S(1)}(t, t') + \sigma_{yx}^{S(2)}(t, t'), \tag{24}$$

where

$$\sigma_{yx}^{Q(1)}(t, t') = \frac{-1}{\omega N}\sum_{\mathbf{k}}\sum_{a,b}\sum_\sigma \frac{\delta v_{ab\sigma}^{(Q)y}(\mathbf{k}, t)}{\delta A_{\text{prob}}^x(t')}G_{b\sigma a\sigma}^<(\mathbf{k}; t, t), \tag{25}$$

$$\sigma_{yx}^{Q(2)}(t, t') = \frac{-1}{\omega N}\sum_{\mathbf{k}}\sum_{a,b}\sum_\sigma v_{ab\sigma}^{(Q)y}(\mathbf{k}, t)\frac{\delta G_{b\sigma a\sigma}^<(\mathbf{k}; t, t)}{\delta A_{\text{prob}}^x(t')}. \tag{26}$$

Then, using the Dyson equation of Green's functions and the Langreth rule[33,47], we obtain

$$\frac{\delta G_{b\sigma a\sigma}^<(\mathbf{k}; t, t)}{\delta A_{\text{prob}}^x(t')}$$
$$= -\sum_{c,d}\sum_{\sigma'} v_{cd\sigma'}^{(C)x}(\mathbf{k}, t')[G_{b\sigma c\sigma'}^R(\mathbf{k}; t, t')G_{d\sigma' a\sigma}^<(\mathbf{k}; t', t)$$
$$+ G_{b\sigma c\sigma'}^<(\mathbf{k}; t, t')G_{d\sigma' a\sigma}^A(\mathbf{k}; t', t)], \tag{27}$$

where $G_{a\sigma b\sigma'}^R(\mathbf{k}; t, t')$ and $G_{a\sigma b\sigma'}^A(\mathbf{k}; t, t')$ are the retarded and advanced Green's functions[34,44,46,47], respectively,

$$G_{a\sigma b\sigma'}^R(\mathbf{k}; t, t') = -i\theta(t - t')\langle\{c_{\mathbf{k}a\sigma}(t), c_{\mathbf{k}b\sigma'}^\dagger(t')\}\rangle, \tag{28}$$

$$G_{a\sigma b\sigma'}^A(\mathbf{k}; t, t') = i\theta(t' - t)\langle\{c_{\mathbf{k}a\sigma}(t), c_{\mathbf{k}b\sigma'}^\dagger(t')\}\rangle. \tag{29}$$

Combining Eq. (27) with Eq. (26), we have

$$\sigma_{yx}^{Q(2)}(t, t') = \frac{1}{\omega N}\sum_{\mathbf{k}}\sum_{a,b,c,d}\sum_{\sigma,\sigma'} v_{ab\sigma}^{(Q)y}(\mathbf{k}, t)v_{cd\sigma'}^{(C)x}(\mathbf{k}, t')$$
$$\times [G_{b\sigma c\sigma'}^R(\mathbf{k}; t, t')G_{d\sigma' a\sigma}^<(\mathbf{k}; t', t)$$
$$+ G_{b\sigma c\sigma'}^<(\mathbf{k}; t, t')G_{d\sigma' a\sigma}^A(\mathbf{k}; t', t)]. \tag{30}$$

Dyson equation of Green's functions. The Green's functions of our periodically driven system are determined from the Dyson equation in a matrix form:

$$G = G_0 + G_0\Sigma G, \tag{31}$$

where G, G_0, and Σ are the matrices of the Green's functions with H_{sb}, those without H_{sb}, and the self-energies due to the second-order perturbation of H_{sb}, respectively,

$$G = \begin{pmatrix} G^R & G^K \\ 0 & G^A \end{pmatrix}, G_0 = \begin{pmatrix} G_0^R & G_0^K \\ 0 & G_0^A \end{pmatrix}, \Sigma = \begin{pmatrix} \Sigma^R & \Sigma^K \\ 0 & \Sigma^A \end{pmatrix}. \tag{32}$$

The superscripts R, A, and K denote the retarded, advanced, and Keldysh components, respectively. For example, the matrix G^R as a function of $\mathbf{k}$ and ω is given by $G^R = ([G_{a\sigma b\sigma'}^R(\mathbf{k}, \omega)]_{mn})$ for $a, b = d_{yz}, d_{zx}, d_{xy}$, $\sigma, \sigma' = \uparrow, \downarrow$, and $m, n = -\infty, \cdots, 0, \cdots, \infty$. The retarded, advanced, and Keldysh components are related to the lesser one through the identity, such as

$$G^< = \frac{1}{2}(G^K - G^R + G^A). \tag{33}$$

By treating the effects of H_{sb} in the second-order perturbation theory, we can express the retarded, advanced, and Keldysh self-energies as follows:

$$[\Sigma_{a\sigma b\sigma'}^R(\mathbf{k}, \omega)]_{mn} = -i\delta_{m,n}\delta_{a,b}\delta_{\sigma,\sigma'}\Gamma, \tag{34}$$

$$[\Sigma_{a\sigma b\sigma'}^A(\mathbf{k}, \omega)]_{mn} = +i\delta_{m,n}\delta_{a,b}\delta_{\sigma,\sigma'}\Gamma, \tag{35}$$

$$[\Sigma_{a\sigma b\sigma'}^K(\mathbf{k}, \omega)]_{mn} = -2i\delta_{m,n}\delta_{a,b}\delta_{\sigma,\sigma'}\Gamma \tanh\frac{\omega + m\Omega}{2T_b}. \tag{36}$$

In deriving them, we have omitted the real parts and replaced $\pi\sum_p V_{pa\sigma}V_{pb\sigma'}\delta(\omega + m\Omega - \epsilon_p + \mu_b)$ by $\Gamma\delta_{a,b}\delta_{\sigma,\sigma'}$ for simplicity. Such simplification may be sufficient because the main effect of H_{sb} is the relaxation towards the nonequilibrium steady state due to the damping[32,33]. Then, using the matrix relation $G^{-1}G = 1$ and Eq. (32), we have

$$(G^R)^{-1} = (G^{-1})^R, \tag{37}$$

$$(G^A)^{-1} = (G^{-1})^A, \tag{38}$$

$$G^K = -G^R(G^{-1})^K G^A, \tag{39}$$

where

$$G^{-1} = \begin{pmatrix} (G^{-1})^R & (G^{-1})^K \\ 0 & (G^{-1})^A \end{pmatrix}. \tag{40}$$

Therefore, the retarded and advanced Green's functions with H_{sb} are obtained by calculating the inverse matrices of $(G^{-1})^R$ and $(G^{-1})^A$, respectively,

$$[(G^{-1})_{a\sigma b\sigma'}^R(\mathbf{k}, \omega)]_{mn} = (\omega + \mu + m\Omega + i\Gamma)\delta_{m,n}\delta_{a,b}\delta_{\sigma,\sigma'}$$
$$- \xi_{ab}^{\sigma\sigma'}\delta_{m,n} - [\epsilon_{ab}(\mathbf{k})]_{mn}\delta_{\sigma,\sigma'}, \tag{41}$$

$$[(G^{-1})_{a\sigma b\sigma'}^A(\mathbf{k}, \omega)]_{mn} = (\omega + \mu + m\Omega - i\Gamma)\delta_{m,n}\delta_{a,b}\delta_{\sigma,\sigma'}$$
$$- \xi_{ab}^{\sigma\sigma'}\delta_{m,n} - [\epsilon_{ab}(\mathbf{k})]_{mn}\delta_{\sigma,\sigma'}, \tag{42}$$

where

$$[\epsilon_{ab}(\mathbf{k})]_{mn} = \int_0^T \frac{dt}{T}e^{i(m-n)\Omega t}\epsilon_{ab}(\mathbf{k}, t). \tag{43}$$

The expressions of $[\epsilon_{ab}(\mathbf{k})]_{mn}$ for our model are provided in Supplementary Note 2; as shown there, $[\epsilon_{ab}(\mathbf{k})]_{mn}$ includes the Bessel functions of the first kind as a function of $u = eA_0$. After obtaining these Green's functions, we can obtain the Keldysh Green's function with H_{sb} by combining Eq. (39) with the following equation:

$$[(G^{-1})_{a\sigma b\sigma'}^K(\mathbf{k}, \omega)]_{mn} = 2i\Gamma\delta_{m,n}\delta_{a,b}\delta_{\sigma,\sigma'}\Gamma \tanh\frac{\omega + m\Omega}{2T_b}. \tag{44}$$

We finally obtain the lesser Green's function with H_{sb} using the three Green's functions obtained and Eq. (33).

Numerical calculations. We numerically calculated Eq. (8) for $Q = C$ or S, σ_{yx}^C or σ_{yx}^S, in the following way. The momentum summation was calculated by dividing the Brillouin zone into a $N_x \times N_y$ mesh and setting $N_x = N_y = 100$. The frequency integral was done by using $\int_{-\Omega/2}^{\Omega/2} d\omega' F(\omega') \approx \sum_{s=0}^{W-1} \Delta\omega' F(\omega'_s)$, where $\omega'_s = -\Omega/2 + s\Delta\omega'$ and $\omega'_W = \Omega/2$, and setting $\Delta\omega' = 0.005$ eV. The frequency derivatives of the Green's functions was approximated by using $\frac{\partial F(\omega')}{\partial \omega'} \approx \frac{F(\omega'+\Delta\omega')-F(\omega'-\Delta\omega')}{2\Delta\omega'}$. The summations over the Floquet indices, $\sum_{m,l,n,q=-\infty}^{\infty}$, was replaced by $\sum_{m,l,n,q=-n_{max}}^{n_{max}}$, and n_{max} was fixed at $n_{max} = 2$ for $\Omega = 6$ and 4 eV or $n_{max} = 3$ for $\Omega = 2$ eV.

Data availability
The data that support the findings of this study are available from the corresponding author upon reasonable request.

Code availability
The code used in the numerical calculations is available from the corresponding author upon reasonable request.

References
1. Shirley, J. H. Solution of the Schrödinger equation with a Hamiltonian periodic in time. *Phys. Rev.* **138**, B979 (1965).
2. Sambe, H. Steady states and quasienergies of a quantum-mechanical system in an oscillating field. *Phys. Rev. A* **7**, 2203 (1973).
3. Bukov, M., D'Alessio, L. & Polkovnikov, A. Universal high-frequency behavior of periodically driven systems: from dynamical stabilization to Floquet engineering. *Adv. Phys.* **64**, 139 (2015).
4. Eckardt, A. Colloquium: atomic quantum gases in periodically driven optical lattices. *Rev. Mod. Phys.* **89**, 011004 (2017).
5. Oka and S. Kitamura, T. Floquet engineering of quantum materials. *Annu. Rev. Condens. Matter Phys.* **10**, 387 (2019).
6. Oka, T. & Aoki, H. Photovoltaic Hall effect in graphene. *Phys. Rev. B* **79**, 081406(R) (2009).
7. Yin, C. M. et al. Observation of the photoinduced anomalous Hall effect in GaN-based heterostructures. *Appl. Phys. Lett.* **98**, 122104 (2011).
8. McIver, J. W. et al. Light-induced anomalous Hall effect in graphene. *Nat. Phys.* **16**, 38–41 (2020).
9. Else, D. V., Bauer, B. & Nayak, C. Floquet time crystals. *Phys. Rev. Lett.* **117**, 090402 (2016).
10. Choi, S. et al. Observation of discrete time-crystalline order in a disordered dipolar many-body system. *Nature* **543**, 221–225 (2017).
11. Zhang, J. et al. Observation of a discrete time crystal. *Nature* **543**, 217–220 (2017).
12. Mentink, J. H., Balzer, K. & Eckstein, M. Ultrafast and reversible control of the exchange interaction in Mott insulators. *Nat. Commun.* **6**, 6708 (2015).
13. Mikhaylovskiy, R. V. et al. Ultrafast optical modification of exchange interactions in iron oxides. *Nat. Commun.* **6**, 8190 (2015).
14. Arakawa, N. & Yonemitsu, K. Floquet engineering of Mott insulators with strong spin-orbit coupling. *Phys. Rev. B* **103**, L100408 (2021).
15. Arakawa, N. & Yonemitsu, K. Polarization-dependent magnetic properties of periodically driven α-RuCl₃. *Phys. Rev. B* **104**, 214413 (2021).
16. Strobel, P. & Daghofer, M. Comparing the influence of Floquet dynamics in various Kitaev-Heisenberg materials. *Phys. Rev. B* **105**, 085144 (2022).
17. Saitoh, E., Ueda, M., Miyajima, H. & Tatara, G. Conversion of spin current into charge current at room temperature: inverse spin-Hall effect. *Appl. Phys. Lett.* **88**, 182509 (2006).
18. Valenzuela, S. O. & Tinkham, M. Direct electronic measurement of the spin Hall effect. *Nature* **442**, 176–179 (2006).
19. Uchida, K. et al. Observation of the spin Seebeck effect. *Nature* **455**, 778–781 (2008).
20. Jaworski, C. M. et al. Observation of the spin-Seebeck effect in a ferromagnetic semiconductor. *Nat. Mater.* **9**, 898–903 (2010).
21. Bauer, G. E. W., Saitoh, E. & van Wees, B. J. Spin caloritronics. *Nat. Mater.* **11**, 391 (2012).
22. Hirsch, J. E. Spin Hall effect. *Phys. Rev. Lett.* **83**, 1834 (1999).
23. Kato, Y. K., Myers, R. C., Gossard, A. C. & Awschalom, D. D. Observation of the spin Hall effect in semiconductors. *Science* **306**, 1910 (2004).
24. Sinova, J., Valenzuela, S. O., Wunderlich, J., Back, C. H. & Jungwirth, T. Spin Hall effects. *Rev. Mod. Phys.* **87**, 1213 (2015).
25. Karplus, R. & Luttinger, J. M. Hall effect in ferromagnetics. *Phys. Rev.* **95**, 1154 (1954).
26. Nagaosa, N., Sinova, J., Onoda, S., MacDonald, A. H. & Ong, N. P. Anomalous Hall effect. *Rev. Mod. Phys.* **82**, 1539 (2010).
27. Claassen, M., Jiang, H.-C., Moritz, B. & Devereaux, T. P. Dynamical time-reversal symmetry breaking and photo-induced chiral spin liquids in frustrated Mott insulators. *Nat. Commun.* **8**, 1192 (2017).
28. Tanaka, T. et al. Intrinsic spin Hall effect and orbital Hall effect in 4d and 5d transition metals. *Phys. Rev. B* **77**, 165117 (2008).
29. Kontani, H., Tanaka, T., Hirashima, D. S., Yamada, K. & Inoue, J. Giant intrinsic spin and orbital Hall effects in Sr₂MO₄ (M = Ru, Rh, Mo). *Phys. Rev. Lett.* **100**, 096601 (2008).
30. Büttiker, M. Small normal-metal loop coupled to an electron reservoir. *Phys. Rev. B* **32**, 1846(R) (1985).
31. Büttiker, M. Role of quantum coherence in series resistors. *Phys. Rev. B* **33**, 3020 (1986).
32. Tsuji, N., Oka, T. & Aoki, H. Nonequilibrium steady state of photoexcited correlated electrons in the presence of dissipation. *Phys. Rev. Lett.* **103**, 047403 (2009).
33. Mikami, T. et al. Brillouin-Wigner theory for high-frequency expansion in periodically driven systems: application to Floquet topological insulators. *Phys. Rev. B* **93**, 144307 (2016).
34. Keldysh, L. V. Diagram technique for nonequilibrium processes. *Zh. Eksp. Teor. Fiz.* **47**, 1515–1527 (1964) [*Sov. Phys. JETP* **20**, 1018–1026 (1965)].
35. Mackenzie, A. P. & Maeno, Y. The superconductivity of Sr₂RuO₄ and the physics of spin-triplet pairing. *Rev. Mod. Phys.* **75**, 657 (2003).
36. Arakawa, N. & Ogata, M. Competition between spin fluctuations in Ca₂₋ₓSrₓRuO₄ around x = 0.5. *Phys. Rev. B* **87**, 195110 (2013).
37. Oguchi, T. Spin-orbit effects on the Ru-d orbital hybridization and Fermi surface in Ca₂₋ₓSrₓRuO₄. *J. Phys. Soc. Jpn.* **78**, 044702 (2009).
38. Damascelli, A. et al. Fermi surface, surface states, and surface reconstruction in Sr₂RuO₄. *Phys. Rev. Lett.* **85**, 5194 (2000).
39. Kirilyuk, A., Kimel, A. V. & Rasing, T. Ultrafast optical manipulation of magnetic order. *Rev. Mod. Phys.* **82**, 2731 (2010).
40. Eckstein, M. & Kollar, M. Theory of time-resolved optical spectroscopy on correlated electron systems. *Phys. Rev. B* **78**, 205119 (2008).
41. Onoda, M., Murakami, S. & Nagaosa, N. Hall effect of light. *Phys. Rev. Lett.* **93**, 083901 (2004).
42. Hosten, O. & Kwiat, P. Observation of the spin Hall effect of light via weak measurements. *Science* **319**, 787 (2008).
43. Kim, M., Lee, D. & Rho, J. Spin Hall effect under arbitrarily polarized or unpolarized light. *Laser Photon. Rev.* **15**, 2100138 (2021).
44. Mahan, G. D. *Many-Particle Physics* (Plenum, New York, 2000).
45. Mizoguchi, T. & Arakawa, N. Controlling spin Hall effect by using a band anticrossing and nonmagnetic impurity scattering. *Phys. Rev. B* **93**, 041304(R) (2016).
46. Kadanoff, L. P. & Baym, G. *Quantum Statistical Mechanics* (Perseus Books, 1989).
47. Rammer, J. & Smith, H. Quantum field-theoretical methods in transport theory of metals. *Rev. Mod. Phys.* **58**, 323 (1986).
48. Kontani, H., Tanaka, T. & Yamada, K. Intrinsic anomalous Hall effect in ferromagnetic metals studied by the multi-d-orbital tight-binding model. *Phys. Rev. B* **75**, 184416 (2007).
49. Arakawa, N. Orbital-cooperative spin fluctuation and orbital-dependent transport in ruthenates. *Phys. Rev. B* **90**, 245103 (2014).
50. D'Alessio, L. & Rigol, M. Long-time behavior of isolated periodically driven interacting lattice systems. *Phys. Rev. X* **4**, 041048 (2014).
51. Dehghani, H., Oka, T. & Mitra, A. Dissipative Floquet topological systems. *Phys. Rev. B* **90**, 195429 (2014).
52. Kawakami, Y., Itoh, H., Yonemitsu, K. & Iwai, S. Strong light-field effects driven by nearly single-cycle 7fs light-field in correlated organic conductors. *J. Phys. B: . Mol. Opt. Phys.* **51**, 174005 (2018).
53. Morota, M. et al. Indication of intrinsic spin Hall effect in 4d and 5d transition metals. *Phys. Rev. B* **83**, 174405 (2011).

Author contributions
N.A. conceived the project, formulated the theory, performed the numerical calculations, and wrote the manuscript. K.Y. supervised the project. All authors discussed the results and commented on the manuscript.

Competing interests
The authors declare no competing interests.

Additional information

Supplementary information The online version contains supplementary material available at https://doi.org/10.1038/s42005-023-01153-9.

Correspondence and requests for materials should be addressed to Naoya Arakawa.

Peer review information *Communications Physics* thanks Tutul Biswas, James LeBlanc and the other, anonymous, reviewer(s) for their contribution to the peer review of this work. Peer reviewer reports are available.

Reprints and permission information is available at http://www.nature.com/reprints

Publisher's note Springer Nature remains neutral with regard to jurisdictional claims in published maps and institutional affiliations.